ChemComm

Surface morphology-induced spin-crossover-inactive high-spin state in a coordination framework

Journal:	*ChemComm*
Manuscript ID	CC-COM-10-2020-006682.R1
Article Type:	Communication

COMMUNICATION

Surface morphology-induced spin-crossover-inactive high-spin state in a coordination framework

Received 00th January 20xx,
Accepted 00th January 20xx

DOI: 10.1039/x0xx00000x

Shun Sakaida,[a] Kazuya Otsubo,*[a] Ken-ichi Otake,[b] Shogo Kawaguchi,[c] Mitsuhiko Maesato,[a] Susumu Kitagawa[b] and Hiroshi Kitagawa*[ab]

Here we report a surface morphology-induced spin state control in ultrathin films of a spin-crossover (SCO) material. The surface microstructure of film domains exhibited selectivity, to stabilize the SCO-active high-spin (HS) or SCO-inactive high-spin (HS2) states. To date, the latter has only been confirmed in the bulk counterpart at gigapascal pressure.

Reaching beyond the size limit of silicon technology is highly desirable for high-density information processing in ultimately miniaturized device dimensions. In this context, molecule-based electronics has attracted a great deal of attention in terms of utilizing the bistability of molecules for switching.[1] Reversible molecular features manipulate the states as binary units by external perturbations such as *cis*–*trans* conformation changes,[2] oxidation–reduction in mixed valence compounds[3] and up–down spin polarization.[4] Among them, the spin-crossover (SCO) phenomenon[5] is a reversible state change observed in $3d^4$–$3d^7$ electron configurations between low-spin (LS, minimum number of unpaired spins) and high-spin (HS, maximum number of unpaired spins) states under external stimuli, e.g., temperature, pressure or light irradiation. SCO sites incorporated into crystalline metal–organic frameworks (MOFs)[6] are known to show a drastic spin transition (cooperative SCO phenomenon coupled to lattice elasticity), accompanied by first-order structural transformation and volume change with a large hysteresis curve, whereas there is a gradual propagation of change in spin state in isolated SCO complexes.[7] Recent progress in findings pertaining to nanoscale crystalline SCO materials is expected to be key to successfully introducing a spin-switching system into a device with high-density integration of functional modules.[8]

The size reduction in SCO materials has been thoroughly discussed in earlier studies; iron (II)-based MOFs were utilized in the form of nanoparticles[9] and thin films,[10] making use of a self-assembled monolayer (SAM). With very few exceptions,[11] most studies on the crystal downsizing effect have revealed that the nature of the multistability of SCO materials is lost in the reduced dimensions. The HS state is, in principle, favoured at reduced crystallite sizes, as reflected by a downshift of transition temperature and an increase in the residual HS fraction at low temperature.[9b] The spin transition becomes relatively incomplete and gradual as the crystal size decreases,[9a] even though there are other factors that also affect the SCO phenomenon (e.g., crystallinity, morphology, elastic interaction at surfaces, and others). Theoretical studies that included use of the core–shell (bulk–surface) model have also revealed that a lower surface energy of a HS state compared with a rigid LS state can be attributed to SCO behaviour at the nanoscale.[12] A loss of transition properties at the nanometre scale stands in stark contrast to the very successful spin-state control at the macroscopic scale (bulk state). Besides a thermally induced HS state, the presence of another HS state has been confirmed in bulk compounds, under limited conditions: light irradiation at <50 K,[13] or gigapascal pressure-induced HS formation.[14]

We have earlier reported a systematic study on the effect of crystal downsizing on structural and physical properties of classic SCO Hofmann-like MOFs $\{Fe(pz)M^{II}(CN)_4\}$ (pz: pyrazine, M = Ni, Pd, Pt)[15a,15b] and $\{Fe(py)_2M^{II}(CN)_4\}$ (**Mpy**, py: pyridine, M = Ni, Pt),[15c–15e] where these compounds show remarkable lattice parameter changes from bulk to film at room temperature (rt). They are therefore expected to show a size-induced spin-state manipulation that is not observed in the bulk state.

Here we report on the effect of surface microstructure on the SCO property using **Nipy** in bulk state (**bulk-Nipy**) and in thin-film form (**film-Nipy**). Magnetic susceptibility data for **bulk-Nipy** recorded in previous studies[16a,16b] indicated that the spin transition occurs at ~190 K; however, its structural transformation accompanied by a change in spin state was not fully identified (it is only reported for the HS structure[16b])

[a] Division of Chemistry, Graduate School of Science, Kyoto University, Kitashirakawa Oiwake-cho, Sakyo-ku, Kyoto 606-8502, Japan.
[b] Institute for Integrated Cell-Material Science (iCeMS), Kyoto University, Yoshida, Sakyo-ku, Kyoto 606-8501, Japan.
[c] Japan Synchrotron Radiation Research Institute (JASRI), SPring-8, 1-1-1 Kouto, Sayo-cho, Sayo-gun, Hyogo, 679-5198, Japan.

† Electronic Supplementary Information (ESI) available: [Experimental details, Rietveld refinement results (CCDC 2030844), variable-temperature Raman spectra and thin-film characterization]. See DOI: 10.1039/x0xx00000x

mainly because of the deterioration of single-crystal quality during its spin transition.

We thus performed a structural investigation using synchrotron powder X-ray diffraction (XRD) analysis of **bulk-Nipy** at 100 K and 298 K (Fig. 1a, Fig. S1, S2 and S6, and Table S1–S3). Rietveld refinement results of **bulk-Nipy** clearly revealed that the spin transition in **bulk-Nipy** is associated with lattice symmetry change (HS: monoclinic, space group *C2/m*, as determined by single-crystal analysis;[16b] LS: orthorhombic, *Cmmm*). This is quite different from the fact that **bulk-Ptpy** lattice symmetry does not change (orthorhombic, space group *Cmmm*) in both spin states.[15e]

We then investigated spin-state monitoring of **bulk-Nipy** by variable-temperature Raman spectroscopy (Fig. 1b and Fig. S3–S5). Unlike in the case of magnetic susceptibility measurements, Raman spectroscopic analysis of the SCO phenomenon[17,18] is applicable for only a few spin sites in a thin film with a thickness of a few nanometres. The spin transition in **bulk-Nipy** can be tracked by Raman shift values of Fe–$N_{pyridine}$ stretching mode,[19] ν(ring) (HS: 1013 cm^{-1}; LS: 1020 cm^{-1}). The HS fraction (γ_{HS}) in Raman spectra was calculated by the value of the HS peak area divided by the area summation of both HS and LS peaks. The HS fraction vs. temperature plot based on Raman spectra (Fig. 1c, right axis) clearly indicated that it is identical with the results of variable-temperature magnetic susceptibility measurement in a field of 0.1 T (left axis). When $T_{1/2}^{down}$ and $T_{1/2}^{up}$ are defined as the transition temperatures, where γ_{HS} is equal to 0.5 in the cooling and heating steps, the temperatures were 205 K and 217 K, respectively.

Having confirmed the applicability of spectroscopic spin-state monitoring to **bulk-Nipy**, we proceeded to investigate the SCO properties of **film-Nipy** fabricated by a liquid-phase layer-by-layer (LbL) assembly protocol (Table S4). Results of previous studies[20] on Hofmann-type MOF thin films have indicated that the surface microstructure plays a key role in controlling the spin state. The degree of coalescence and interparticle interaction in a **Ptpy** LbL film was suggested to be linked to SCO behaviour in ultrathin films,[20] and hence the control of morphology in **film-Nipy** is expected to display changes in spin transition properties.

To investigate a morphology effect on SCO behaviour in nanofilms, LbL films were deposited on a substrate, applying two different pretreatment conditions of the Au surface (with/without thermal annealing). For both conditions, LbL crystal growth reached to a similar film thickness at the same cycle number, confirmed by infrared reflection absorption spectroscopy (IRRAS, Fig. S7) and atomic force microscopy (AFM, Fig. S8). The microstructure of the fabricated films was observed by AFM using tapping mode (Fig. 2 and Fig. S9). Topographic AFM images in Fig. 2 revealed that the thermal pretreatment of the Au surface has a significant effect on the subsequent thin-film growth. The crystal domain size of **film-Nipy** on an annealed Au substrate was almost twice as large as that on an as-supplied Au substrate for both **film-Nipy-20L** and **film-Nipy-40L** (20 and 40 LbL cycles, respectively, see Fig. S11 and S12). This was possibly derived from necking domains of the Au surface with lower roughness (Fig. S10 and S21), induced by the annealing treatment. Surface XRD profiles also indicated high crystallinity and larger crystallite size of **film-Nipy** on annealed Au substrate (Fig. S19 and S20). Consequently, we monitored the spin state of fabricated films on an Au substrate with/without H_2 annealing using variable-temperature Raman spectroscopy measurements. An

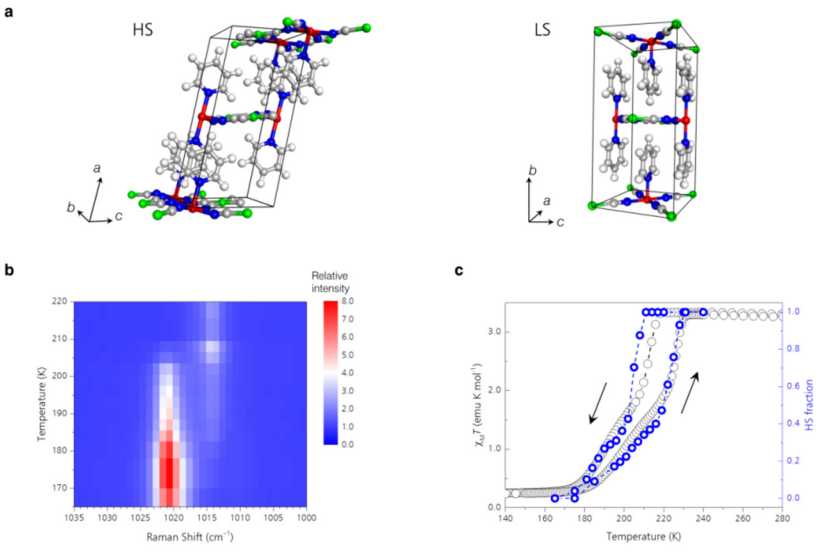

Fig. 1 Spin transition accompanied by structural transformation in **bulk-Nipy**. (a) A perspective view of the unit cell for **bulk-Nipy** in (left) HS and (right) LS states. Colour code: Fe (red), C (grey), H (white), N (blue), Ni (green). A full dataset of crystal structure is shown in the ESI. (b) Normalized intensity of variable-temperature Raman spectra for **bulk-Nipy** ν(ring) mode in the cooling step. The colour scale indicates the intensity ratio to the intensity at 1000 cm^{-1} at each temperature. (c) SCO behaviour observed in **bulk-Nipy**. Magnetic susceptibility (left axis, black open circles) exhibited transition curves with thermal hysteresis, in agreement with the results of Raman spectra monitoring (right axis, blue open circles). Black arrows represent the sweeping directions of temperature.

intriguing size and morphology effect on the SCO properties of **Nipy** was confirmed (Fig. 3a and Fig. S13–S15), as observed in data for **film-Nipy** using different substrate treatments. Raman spectra of *ν*(ring) mode in Fig. 3a indicated that the spin state observed in **film-Nipy-20L** on an annealed Au substrate was ascribed neither to the HS state (around 1013 cm^{-1}) nor the LS state (around 1020 cm^{-1}), and the peak was observed at an intermediate point (around 1016 cm^{-1}). Based on earlier observations by Molnár *et al.*,[18] we assigned it to the peak from the SCO-inactive HS (HS2) state because no change in spin state from HS2 was confirmed in the experimental temperature range from 150 K to the film decomposition temperature of <400 K (see Fig. 3b and Fig. S13, S17 and S18). Furthermore, Raman spectra provided evidence that an in-plane ring deformation mode (ν_{6a}, Fig. S16) was not seen in this state, which was used as an indicator of the LS state in an earlier study.[18]

Fig. 4 shows spin transition curves of **film-Nipy** and **bulk-Nipy**. For **film-Nipy** on an as-supplied Au substrate (SCO active), a typical downsizing effect on SCO behaviour was observed. The $T_{1/2}$ shifted lower as the crystal size decreased and a residual HS state (~10%) was observed at 150 K. Unlike SCO behaviour in **film-Ptpy**,[15e] the hysteresis almost diminished in **film-Nipy**. On the other hand, **film-Nipy-20L** and **film-Nipy-40L** on annealed Au substrate were SCO inactive over the measured temperature. These results suggest that the surface microstructure of domains in Fig. 2 reflects the stabilized spin state in thin-film form. Crystal domains of **Nipy** on annealed Au substrate were found to be highly aggregated in comparison with coarse granular-like particles on the as-supplied substrate, reflected by surface roughness parameters (Fig. S22) Interestingly, the HS2 state has been observed in **bulk-Nipy** as a result of an unusual LS→HS reverse transition under high pressure (3–5 GPa).[18] Furthermore, the observed *ν*(CN) peak in **film-Nipy** at rt (Fig. 3a and Fig. S13) exhibited a broadening, with a blue shift, similar to what has been reported earlier in pressure-induced experiments.[18] The peak position of *ν*(CN) modes is known to be proportional to the applied pressure (~2 GPa) in several transition metal cyanide compounds.[21,22] The findings of earlier works suggest that the application of an external pressure has the effect of strengthening the ligand field, to first stabilize the LS state, and this is followed by the appearance of the HS2 state at a much higher pressure region, probably due to (irreversible) structural change caused by compression. It should be noted that the axial compression of the octahedral structure has also been proposed for a minor component of the HS2 state in other Hofmann-like MOFs.[23] The local coordination environment in the HS2 state was similar to that in the SCO-inactive $FeN_4(OH_2)_2$ core, confirmed by ^{57}Fe Mössbauer parameters.[23] We also performed density functional theory (DFT) calculation at the BP86/def2-TZVP level of theory for a simplified model on $FeN_4(py)_2$ core, suggesting the axially-compressed structure in HS2 state (Fig. S23 and S24).

In summary, we investigated surface morphology effect on the SCO phenomenon in a crystalline coordination framework $\{Fe(py)_2[Ni(CN)_4]\}$ using two different surface conditions of the substrate. Variable-temperature Raman spectroscopy demonstrated a clear difference in spin-state stabilization at the nanoscale, comparing typical HS state preference and SCO-inactive HS2 state appearance. AFM observations revealed that stabilization of the HS2 state is derived from the surface morphology of densely packed crystal domains. A crystal

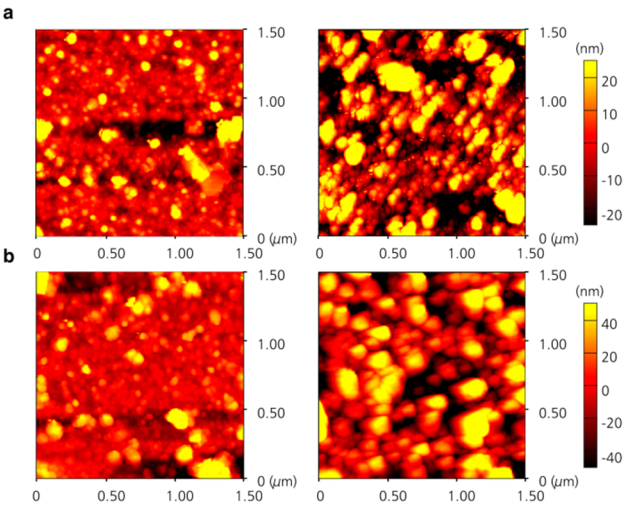

Fig. 2 Surface morphology of the fabricated films. Topographic AFM images were collected using tapping mode for (a) **film-Nipy-20L** and (b) **film-Nipy-40L** grown on a SAM-anchored Au(111) surface. Pretreatment of Au substrate: (left) none—substrate used as supplied, (right) H_2 annealed.

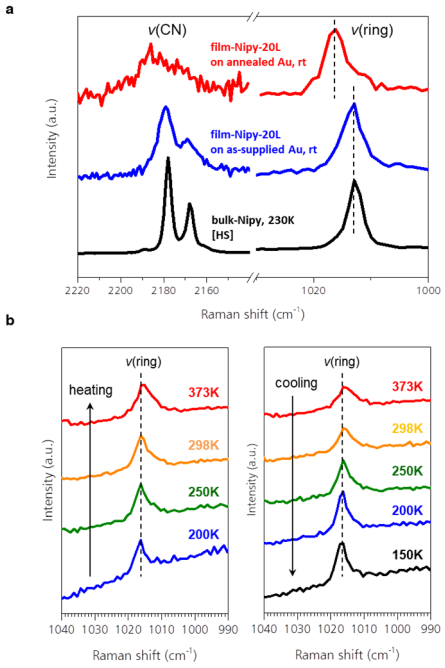

Fig. 3 Different size reduction effects on the stabilized spin state. (a) Raman spectra of *ν*(CN) and *ν*(ring) modes of (black) **bulk-Nipy** in HS state and **film-Nipy-20L** at rt on (red) annealed and (blue) as-supplied Au substrate. (b) Variable temperature Raman spectra of **film-Nipy-20L** on annealed Au substrate. No spin-state change from HS2 was observed.

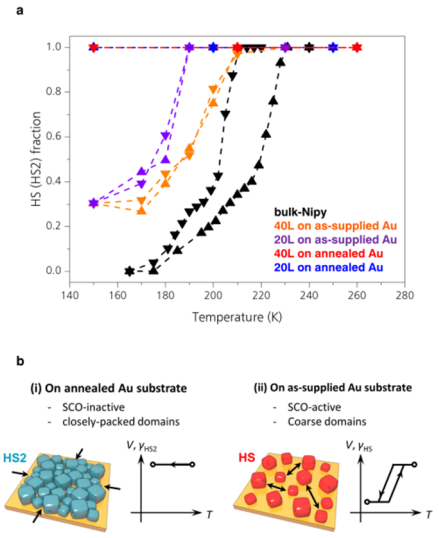

Fig. 4 Spin-crossover behaviour in ultrathin films. (a) Spin transition curves plotted against temperature for **bulk-Nipy** and **film-Nipy** on as-supplied/annealed Au substrate. Triangles and inverted triangles denote heating and cooling processes, respectively. (b) Surface microstructure-driven spin state of films in (i) HS2 and (ii) HS states.

downsizing strategy presented here allowed us to characterize the HS2 state at ambient conditions, in contrast with the HS2 state as a high-pressure phase in the bulk state. The insight that emanated from this study should be helpful towards accelerating nanomaterial implementation into spin-driven devices.

This work was supported by Core Research for Evolutional Science and Technology (CREST) 'Creation of Innovative Functions of Intelligent Materials on the Basis of the Element Strategy', ACCEL from Japan Science and Technology Agency (JST), Grant-in-Aid for Specially Promoted Research (20H05623), and JSPS KAKENHI Grant Numbers JP20350030, JP23245012, JP15H05479, JP17H05366, JP19K05494 and JP19H04572 (Coordination Asymmetry). Synchrotron XRD measurements were performed at SPring-8, supported by the Japan Synchrotron Radiation Research Institute (JASRI) (Proposal Nos. 2017A1415, 2018B1138 and 2019B1387).

Conflicts of interest

There are no conflicts of interest to declare.

References

1 A. Von Hippel, *Molecular Science and Molecular Engineering*, The Technology Press of M.I.T. and John Wiley & Sons, New York, 1959.
2 C. Dri, M. V. Peters, J. Schwarz, S. Hecht and L. Grill, *Nature Nanotechnol*., 2008, **3**, 649.
3 J. Jiao, G. J. Long, L. Rebbouh, F. Grandjean, A. M. Beatty and T. P. Fehlner, *J. Am. Chem. Soc*., 2005, **127**, 17819.
4 K. V. Raman, A. M. Kamerbeek, A. Mukherjee, N. Atodiresei, T. K. Sen, P. Lazić, V. Caciuc, R. Michel, D. Stalke, S. K. Mandal, and S. Blügel, *Nature*, 2013, **493**, 509.
5 (a) L. Cambi and L. Szegö, *Ber. Dtsch. Chem. Ges*., 1931, **64**, 2591. (b) A. Bousseksou, G. Molnár, L. Salmon and W. Nicolazzi, *Chem. Soc. Rev*., 2011, **40**, 3313. (c) O. Kahn and C. J. Martinez, *Science*, 1998, **279**, 44.
6 (a) Z. P. Ni, J. L. Liu, M. N. Hoque, W. Liu, J. Y. Li, Y. C. Chen and M. L. Tong, *Coord. Chem. Rev*., 2017, **335**, 28. (b) R. Ohtani and S. Hayami, *Chem. A Eur. J*., 2017, **23**, 2236. (c) M. Nakaya, R. Ohtani and S. Hayami, *Eur. J. Inorg. Chem*., 2020, **39**, 3709.
7 J. A. Real, A. B. Gaspar and M. C. Muñoz, *Dalton Trans*., 2005, **12**, 2062.
8 (a) G. Molnár, S. Rat, L. Salmon, W. Nicolazzi and A. Bousseksou, *Adv. Mater*., 2018, **30**, 17003862. (b) K. Otsubo, T. Haraguchi and H. Kitagawa, *Coord. Chem. Rev*., 2017, **346**, 123. (c) H. J. Shepherd, G. Molnár, W. Nicolazzi, L. Salmon and A. Bousseksou, *Eur. J. Inorg. Chem*., 2013, **5**, 653. (d) C. Lefter, V. Davesne, L. Salmon, G. Molnár, P. Demont, A. Rotaru and A. Bousseksou, *Magnetochemistry*, 2016, **2**, 18. (e) V. Rubio-Giménez, S. Tatay and C. Martí-Gastaldo, *Chem. Soc. Rev*., 2020, **49**, 5601. (f) K. S. Kumar and M. Ruben, *Coord. Chem. Rev*., 2017, **346**, 176.
9 (a) F. Volatron, L. Catala, E. Rivière, A. Gloter, O. Stéphan and T. Mallah, *Inorg. Chem*., 2008, **47**, 6584. (b) I. Boldog, A. B. Gaspar, V. Martínez, P. Pardo-Ibañez, V. Ksenofontov, A. Bhattacharjee, P. Gütlich and J. A. Real, *Angew. Chem. Int. Ed*., 2008, **47**, 6433.
10 (a) M. Cavallini, *Phys. Chem. Chem. Phys*., 2012, **14**, 11867. (b) V. Rubio-Giménez, G. Escorcia-Ariza, C. Bartual-Murgui, C. Sternemann, M. Galbiati, J. Castells-Gil, J. A. Real, S. Tatay and C. Marti-Gastaldo, *Chem. Mater*., 2019, **31**, 7277.
11 H. Peng, S. Tricard, G. Félix, G. Molnár, W. Nicolazzi, L. Salmon and A. Bousseksou, 2014. *Angew. Chem. Int. Ed*., 2014, **53**, 10894.
12 A. Muraoka, K. Boukheddaden, J. Linarès and F. Varret, *Phys. Rev. B*, 2011, **84**, 054119.
13 S. Decurtins, P. Gütlich, C. P. Köhler, H. Spiering and A. Hauser, *Chem. Phys. Lett*., 1984, **105**, 1–4.
14 O. Troeppner, R. Lippert, T. E. Shubina, A. Zahl, N. Jux and I. Ivanović-Burmazović, *Angew. Chem. Int. Ed*., 2014, **53**, 11452.
15 (a) K. Otsubo, T. Haraguchi , O. Sakata, A. Fujiwara and H. Kitagawa, *J. Am. Chem. Soc*., 2012, **134**, 9605. (b) T. Haraguchi, K. Otsubo and H. Kitagawa, *Eur. J. Inorg. Chem*., 2018, **16**, 1697. (c) S. Sakaida, K. Otsubo, O. Sakata, C. Song, A. Fujiwara, M. Takata and H. Kitagawa, *Nature Chem*., 2016, **8**, 377. (d) S. Sakaida, T. Haraguchi, K. Otsubo, O. Sakata, A. Fujiwara and H. Kitagawa, *Inorg. Chem*., 2017, **56**, 7606. (e) S. Sakaida *et al. Inorg. Chem*., 2020, in press.
16 (a) V. Niel, J. M. Martinez-Agudo, M. C. Munoz, A. B. Gaspar and J. A. Real, *Inorg. Chem*., 2001, **40**, 3838. (b) T. Kitazawa, Y. Gomi, M. Takahashi, M. Takeda, M. Enomoto, A. Miyazaki and T. Enoki, *J. Mater. Chem*., 1996, **6**, 119.
17 S. Cobo, G. Molnár, J. A. Real and A. Bousseksou, *Angew. Chem. Int. Ed*., 2006, **45**, 5786.
18 G. Molnár, T. Kitazawa, L. Dubrovinsky, J. J. McGarvey and A. Bousseksou, *J. Phys. Condens. Matter*, 2004, **16**, S1129.
19 S. Akyüz, A. B. Dempster, R. L. Morehouse and S. Suzuki, *J. Mol. Struct*., 1973, **17**, 105.
20 V. Rubio-Giménez, C. Bartual-Murgui, M. Galbiati, A. Núñez-López, J. Castells-Gil, B. Quinard, P. Seneor, E. Otero, P. Ohresser, A. Cantarero and E. Coronado, *Chem. Sci*., 2019, **10**, 4038.
21 (a) G. J. Long and B. B. Hutchinson, *Inorg. Chem*., 1987, **26**, 608. (b) Y. Garcia, V. Ksenofontov, G. Levchenko, G. Schmitt and P. Gütlich, *J. Phys. Chem. B*, 2000, **104**, 5045. (c) G. Molnár, V. Niel, J. A. Real, L. Dubrovinsky, A. Bousseksou and J. J. McGarvey, *J. Phys. Chem. B*, 2003, **107**, 3149.
22 Y. Moritomo, T. Matsuda, R. Fuchikawa, Y. Abe and H. Kamioka, *J. Phys. Soc. Jpn*., 2011, **80**, 024603.
23 T. Kitazawa, M. Sekiya, T. Kawasaki and M. Takahashi, *Hyperfine Interact*., 2016, **237**, 29.

We report crystal size and morphology effects on the spin-crossover phenomenon in ultrathin films of a classic Hofmann-like metal–organic framework, $\{Fe(py)_2Ni(CN)_4\}$. Variable-temperature Raman spectroscopy revealed a clear difference in spin-state stabilization at the nanoscale, comparing typical high-spin state preference and spin-crossover-inactive high-spin state appearance.

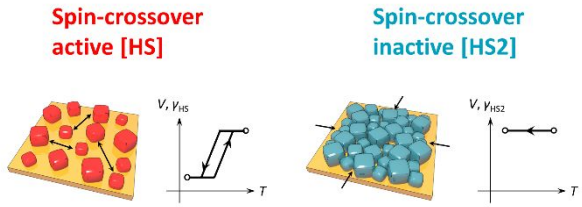

TOC image

ORCID information for Authors

Mr. Shun Sakaida: 0000-0002-4172-1598

Dr. Kazuya Otsubo: 0000-0003-4688-2822

Dr. Ken-ichi Otake: 0000-0002-7904-5003

Dr. Shogo Kawaguchi: 0000-0002-8498-0936

Dr. Mitsuhiko Maesato: 0000-0001-6675-0531

Prof. Susumu Kitagawa: 0000-0001-6956-9543

Prof. Hiroshi Kitagawa: 0000-0001-6955-3015

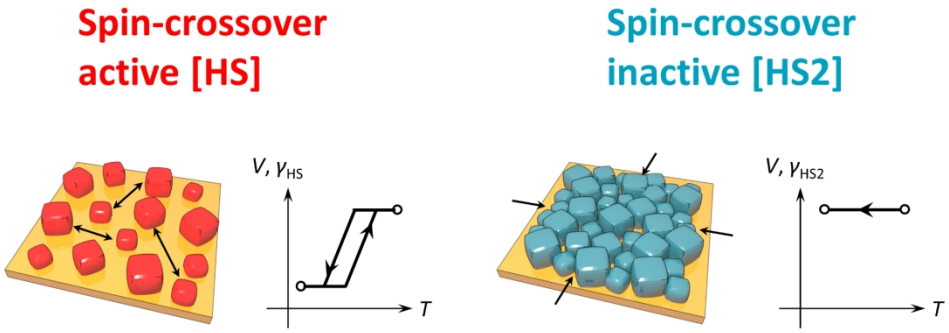

80x30mm (600 x 600 DPI)